Alexandria Engineering Journal (2016) 55, 2405–2421

HOSTED BY

Alexandria University

Alexandria Engineering Journal

www.elsevier.com/locate/aej
www.sciencedirect.com

ORIGINAL ARTICLE

Thermal radiation energy on squeezed MHD flow of Cu, Al_2O_3 and CNTs-nanofluid over a sensor surface

Nor Shamsidah bte Amir Hamzah, R. Kandasamy *, Radiah Muhammad

Research Centre for Computational Mathematics, FSTPi, Universiti Tun Hussein Onn Malaysia, 86400 Parit Raja, Batu Pahat, Johor, Malaysia

Received 16 December 2015; revised 8 April 2016; accepted 12 April 2016
Available online 13 May 2016

KEYWORDS

Nanofluids;
Squeezed flow;
Heat transfer;
Sensor surface;
CNTs;
Thermal radiation energy

Abstract The squeezed MHD flow of water, ethylene glycol and engine oil based metallic nanoparticles over a sensor surface in the presence of thermal radiation energy have been investigated. The physical significance of the problem is water, ethylene glycol and engine oil based on the geometry and the interaction of copper (Cu), alumina (Al_2O_3) and carbon nanotubes (SWCNTs and MWCNTs). The governing partial differential equations of momentum and energy are transformed to similarity equations (ODEs) for certain families of the controlling parameters. The numerical and analytical solutions of the resulting ODEs are solved using fourth or fifth order Fehlberg method with shooting technique and optimal homotopy asymptotic method (OHAM) and it is also found that there is no significance difference between them. It is investigated that in squeezing flow phenomena, SWCNTs-engine oil in the presence of thermal radiation energy gives approximately more than 30% enhancement in the heat transfer as compared to the water based SWCNTs and MWCNTs.

1. Introduction

Physical and biological situations associate the channels with expanding and contracting walls. Cleansing chambers in industries, respiratory system in organisms, aerospace engineering, coolant circulation, filling machines and inter-body fluid transportation are some of these situations. Due to these applications, the researchers are interested to analyze the problems related to these kinds of flows. A number of studies are accessible casting light on various aspects of the flows through channels with dilating/squeezing walls. To upgrade the physical and thermal properties of poor conducting fluids, nanotechnology has shown some ways. By mixing nano-scaled metal particles, the properties such as conduction can be boosted. These enrichments can lead to better and more advanced mechanical and thermal systems. The idea of mixing macro–micro sized metal particles to the fluids/coolants inherently poor conductors of heat transfer, was introduced by many authors [1–6].

Nanofluid flow within the squeezed surface could be a new energy source. Squeeze flows are flows in which material nanoparticles are compressed between two parallel plates

* Corresponding author.
E-mail address: future990@gmail.com (R. Kandasamy).
Peer review under responsibility of Faculty of Engineering, Alexandria University.

http://dx.doi.org/10.1016/j.aej.2016.04.019

Nomenclature

B_0	magnetic flux density ($\mathrm{kg\ s^{-2}\ A^{-1}}$)
CNT	carbon nanotubes
c_p	specific heat at constant pressure ($\mathrm{J\ kg^{-1}\ K^{-1}}$)
k^*	mass absorption coefficient ($\mathrm{m^{-1}}$)
K	permeability of the porous medium ($\mathrm{m^2}$)
k_f	thermal conductivity of the base fluid ($\mathrm{W\ m^{-1}\ K^{-1}}$)
k_s	thermal conductivity of the nanoparticle ($\mathrm{W\ m^{-1}\ K^{-1}}$)
k_{nf}	effective thermal conductivity of the nanofluid ($\mathrm{W\ m^{-1}\ K^{-1}}$)
Pr	Prandtl number, $\frac{\nu_f}{\alpha_f}\left(\frac{\mathrm{m^2\ s^{-1}}}{\mathrm{m^2\ s^{-1}}}\right)$ (–)
M	magnetic parameter, $\frac{\sigma B_0^2 x}{U\rho_f}$, $\left(\frac{\Omega^{-1}\ \mathrm{m^{-1}} B_0^2 m}{\mathrm{m\ s^{-1}\ kg\ m^{-3}}}\right)$ (–)
MHD	magnetohydrodynamics
MWCNT	multiwall carbon nanotubes
OHAM	optimal homotopy asymptotic method
q''_{rad}	incident radiation flux of intensity ($\mathrm{kg\ m^{-1}\ s^{-3}\ K^{-1}}$)
Q_0	rate of source/sink ($\mathrm{kg\ m^{-2}}$)
SWCNT	single wall carbon nanotubes
t	time (s)
T	temperature of the fluid (K)
T_w	temperature of the wall (K)
T_∞	temperature of the fluid far away from the wall (K)
R	thermal radiation parameter, $\frac{16\sigma_1 T_w^3}{3k_f k^*} = \left(\frac{\mathrm{kg\ s^{-3}\ K^{-4}\ K^3}}{\mathrm{kg\ m\ s^{-3}\ K^{-1}\ m^{-1}}}\right)$ (–)
u, v	velocity components in x and y direction ($\mathrm{m\ s^{-1}}$)
$U(x)$	flow velocity of the fluid away from the wedge ($\mathrm{m\ s^{-1}}$)
V_0	velocity of suction/injection ($\mathrm{m\ s^{-1}}$)

Greek symbols

α_{nf}	thermal diffusivity of the nanofluid ($\mathrm{m^2\ s^{-1}}$)
ρ_f	density of the base fluid ($\mathrm{kg\ m^{-3}}$)
ρ_s	density of the nanoparticle ($\mathrm{kg\ m^{-3}}$)
ρ_{nf}	effective density of the nanofluid ($\mathrm{kg\ m^{-3}}$)
$(\rho c_p)_{nf}$	heat capacitance of the nanofluid ($\mathrm{J\ m^{-3}\ K^{-1}}$)
σ_{nf}	electric conductivity of the nanofluid ($\mathrm{\Omega^{-1}\ m^{-1}}$)
σ_1	Stefan–Boltzmann constant ($\mathrm{kg\ s^{-3}\ K^{-4}}$)
μ_f	dynamic viscosity of the base fluid ($\mathrm{kg\ m^{-1}\ s^{-1}}$)
μ_{nf}	effective dynamic viscosity of the nanofluid ($\mathrm{kg\ m^{-1}\ s^{-1}}$)
ν_{nf}	dynamic viscosity of the nanofluid ($\mathrm{m^2\ s^{-1}}$)
δ	heat source/sink parameter, $\frac{Q_0 x}{(\rho c_p)_f U}$, $\left(\frac{\mathrm{kg\ m^{-1}\ s^{-3}\ K^{-1}\ m}}{\mathrm{kg\ m^{-2}\ s^{-1}\ (m^2\ s^{-2}\ K^{-1})}}\right)$ (–)
λ	porous parameter, $\frac{\nu_f x}{KU}\left(\frac{\mathrm{m^2\ s^{-1} m}}{\mathrm{m\ m^2\ s^{-1}}}\right)$ (–)
ζ	nanoparticle volume fraction (–)
ψ	dimensionless stream function (–)
η	similarity variable (–)
f	dimensionless stream function (–)
θ	dimensionless stream function (–)

and thus squeezed out radially. Practical applications of squeezing flows in these fields are polymer processing, modeling of lubrication systems, and compression and injection molding and also squeezing flow under the influence of magnetic field has many applications in the field of chemical engineering and it is experimented by many researchers [7–14]. Verma [15] and Singh et al. [16] studied the simulation solutions of the squeezing flows between parallel plates. Leider and Bird [17] explained the theoretical analysis for squeezing flow of power-law fluid between parallel plates. Naduvinamani et al. [18] analyzed the squeeze film lubrication of a short porous journal with couple stress fluids. The study of the porosity and squeezing effects, while studying the unsteady squeezing flow of visco-elastic Jeffery fluid between parallel disks, has been prepared by Qayyum et al. [19]. Apart from the mentioned scholars, other researchers have also investigated the different theoretical and experimental studies of squeezing flows and many chemical and biological sensors involve extending surfaces as their sensing elements [20–23].

The use of carbon nanotube suspension in fluids received appreciable attention due to practical benefits; large surface area, high mobility and less particle momentum are some of the benefits. The conventional heat transfer fluids, such as engine oil, ethylene glycol and water have poor thermal conductivity as compared to solids. To enhance the thermal conductivity of such fluids, nanoparticles of copper, alumina and carbon nanotubes having higher thermal conductivity are integrated within the base fluid which provides the better heat transfer rate. As far as conduction is concerned, for engine oil, it can be upgraded up to 20,000 times at room temperature by utilizing multi-walled carbon nanotubes (MWCNTs) [24]. Iijima [25] suggested an idea of nanoparticles based on carbon nanotubes (CNTs) to be used in various devices such as solar cells and ultra-capacitors. CNTs can further be divided into different categories on the basis of their structural traits. Two of them are single-walled and multi-walled carbon nanotubes (SWCNTs and MWCNTs). The details about their structure found in [26–41] are the studies describing the use of nanofluids in diversified geometries and situations. Squeezing flow between parallel plates is a fascinating area of research as it occurs in numerous applications in science and engineering which include hydro dynamical machines, polymer processing, chemical processing equipment, formation and dispersion of fog, damage of crops due to freezing, compression, transient loading of mechanical components, injection modeling and the squeezed films in power transmission.

The objective of the present work was to analyze the effects of Copper, Alumina and CNTs suspended in water, ethylene glycol and engine oil based unsteady external squeezing MHD flow over a horizontal permeable sensor surface in the presence of thermal radiation energy. The obtained governing nonlinear partial differential equations are transformed to nonlinear ordinary differential equations by using the similarity transformation and afterward the problem is solved by applying the fourth or fifth order Runge–Kutta Fehlberg method with shooting technique and OHAM. Several aspects of the problem are investigated and shown graphically with

respect to the physical parameters involved in it and the current outputs are compared with the available literature.

2. Mathematical analysis

The unsteady and heat transfer in a two-dimensional MHD squeezing nanofluid flow between two infinite parallel plates is designed in this work. Physical flow configuration of the problem is fixed in such a way that the plate is enclosed inside a squeezed channel such that the height $h(t)$ is higher than the boundary layer thickness and the squeezing in the free stream is studied to start from the tip of the surface as presented in Fig. 1. Micro-cantilever sensor is placed between the plates and the upper plate is squeezed while lower plate is fixed. The working nanofluid is appropriated to be Newtonian and electrically conducting with σ as its electrical conductance and the magnetic field with a time-dependent strength B_0 is activated normal to the flow in the y-direction whereas the induced magnetic Reynolds number is negligible. The continuity, momentum and energy governing equations are defined [42,43] as

$$\frac{\partial u}{\partial x}+\frac{\partial v}{\partial y}=0 \tag{1}$$

$$\frac{\partial u}{\partial t}+u\frac{\partial u}{\partial x}+v\frac{\partial u}{\partial y}=-\frac{1}{\rho_{nf}}\left(\frac{\partial p}{\partial x}\right)+\frac{\mu_{nf}}{\rho_{nf}}\left(\frac{\partial^2 u}{\partial y^2}\right)-\left(\frac{\mu_{nf}}{\rho_{nf}K}+\frac{\sigma_{nf}B_0^2}{\rho_{nf}}\right)u \tag{2}$$

$$\frac{\partial U}{\partial t}+U\frac{\partial U}{\partial x}=-\frac{1}{\rho_{nf}}\left(\frac{\partial p}{\partial x}\right)-\frac{\sigma_{nf}B_0^2}{\rho_{nf}}U \tag{3}$$

$$\frac{\partial T}{\partial t}+u\frac{\partial T}{\partial x}+v\frac{\partial T}{\partial y}=\alpha_{nf}\frac{\partial^2 T}{\partial y^2}-\frac{1}{(\rho c_p)_{nf}}\frac{\partial q_r}{\partial y}+\frac{Q_0(T-T_\infty)}{(\rho c_p)_{nf}} \tag{4}$$

with boundary conditions

$$u(x,0,t)=0,\ v(x,0,t)=v_0(t),-k_{nf}\frac{\partial T(x,0,t)}{\partial t}=q(x),$$
$$u(x,\infty,t)=U(x,t),T(x,\infty,t)=T_\infty \tag{5}$$

u, v – the velocity component in the x and y directions, T – the temperature of the nanofluid, t – time, p – the fluid pressure, σ_s, σ_f – the electrical conductivity of the base fluid and the nanofluid, v_0 – a constant. Physically, $v_w<0$ means injection and $v_w>0$ implies suction of fluid, U – the free-stream velocity, a is a constant, and Q_0 – heat generation or absorption coefficient. The magnetic Reynolds number is considered small such that the magnetic boundary-layer thickness is large and the induced magnetic field is imperceptible compared with the applied magnetic field.

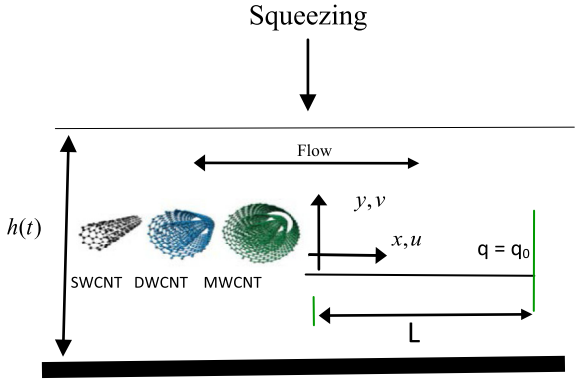

Figure 1 Flow configuration and coordinate system.

Convective heat transfer can be enhanced passively by changing flow geometry, boundary conditions, or by enhancing thermal conductivity and viscosity of the fluid. Various techniques have been proposed to enhance the heat transfer performance of fluids. Researchers have also tried to increase the thermal conductivity and viscosity of base fluids by suspending micro- or larger-sized solid particles in fluids, since the thermal conductivity of solid is typically higher than that of liquids. Numerous theoretical and experimental studies of suspensions containing solid particles have been conducted since Maxwell's theoretical work was published more than 100 years ago. Currently, there is no reliable theory to predict the anomalous thermal conductivity and viscosity of nanofluids. From the experimental results of many researchers, it is known that the thermal conductivity and viscosity of nanofluids depend on parameters including the thermal conductivity and viscosity of the base fluid and the nanoparticles, the volume fraction, the surface area, the shape of the nanoparticles and the temperature. There are no theoretical formulas currently available to predict the thermal conductivity and viscosity of nanofluids satisfactorily. For particle–fluid mixtures, numerous theoretical studies have been conducted dating back to the classical work of Maxwell [44,45]. The Maxwell model for thermal conductivity for solid–liquid mixtures of relatively large particles (micro-/mini-size) is good for low solid concentrations. Viscosity describes a fluid internal resistance to flow and, in the case of nanofluids, depends on the morphology and size of nanoparticles. Based on the nanofluid thermophysical properties, k_{nf} – the thermal conductivity of the nanofluid, α_{nf} – the effective thermal diffusivity of the nanofluid, ρ_{nf} – the effective density of the nanofluid, μ_{nf} – the effective dynamic viscosity of the nanofluid, σ_{nf} – the electrical conductivity of the nanofluid and $(\rho c_p)_{nf}$ – specific heat of the nanofluid, are defined as

$$\alpha_{nf}=\frac{k_{nf}}{(\rho c_p)_{nf}},\ \rho_{nf}=(1-\zeta)\rho_f+\zeta\rho_s,\ \mu_{nf}=\frac{\mu_f}{(1-\zeta)^{2.5}},$$
$$\times(\rho c_p)_{nf}=(1-\zeta)(\rho c_p)_f+\zeta(\rho c_p)_s,$$
$$\sigma_{nf}=(1-\zeta)\sigma_f+\zeta\sigma_s,\ \frac{k_{nf}}{k_f}=\left\{\frac{(k_s+2k_f)-2\zeta(k_f-k_s)}{(k_s+2k_f)+2\zeta(k_f-k_s)}\right\} \tag{6}$$

where ζ is the nanoparticle volume fraction, μ_f is the dynamic viscosity of the base fluid, β_f and β_s are the volumetric expansion coefficients of the base fluid and nanoparticle, respectively, ρ_f and ρ_s are the density of the base fluid and nanoparticle, σ_f and σ_s are the electric conductivity of the base fluid and nanoparticle, k_f – the thermal conductivity of the fluid, and k_s – the thermal conductivity of the solid fraction. Applying Rosseland approximation $q''_{rad}=q_r=-\frac{4\sigma_1}{3k^*}\frac{\partial T^4}{\partial y}$ [46], σ_1 – Stefan–Boltzmann constant, and k^* – mean absorption coefficient. By Taylor's series expansion of T^4 being

$$T^4\cong 4T_\infty^3T-3T_\infty^4.\ \frac{\partial q_r}{\partial y}=-\frac{16\sigma_1T_\infty^3}{3k^*}\frac{\partial^2T}{\partial y^2}$$

Based on the free-stream condition, Eqs. (2) and (3) become

Table 1 Thermophysical properties of the fluid and nanoparticles.

	ρ (kg/m^3)	c_p (J/kg K)	k (W/m K)
Pure water	997.1	4179	0.613
Ethylene glycol	1115	2430	0.253
Engine oil	884	1910	0.144
Copper (Cu)	8933	385	401
Alumina (Al_2O_3)	3970	765	40
SWCNTs	2600	425	6600
MWCNTs	1600	796	3000

$$\frac{\partial u}{\partial t}+u\frac{\partial u}{\partial x}+v\frac{\partial u}{\partial y}=\frac{\partial U}{\partial t}+U\frac{\partial U}{\partial x}+\frac{\mu_{nf}}{\rho_{nf}}\frac{\partial^2 u}{\partial y^2}-\left(\frac{\mu_{nf}}{\rho_{nf}K_0}+\frac{\sigma_{nf}B_0^2}{\rho_{nf}}\right)(u-U) \tag{7}$$

where $U\frac{dU}{dx}=-\frac{1}{\rho_{nf}}\frac{\partial P}{\partial x}-\left(\frac{\mu_{nf}}{\rho_{nf}K_0}+\frac{\sigma_{nf}B_0^2}{\rho_{nf}}\right)U$, K – non-uniform permeability of the medium, B_0 – the externally imposed magnetic field in the y-direction. The stream function satisfying Eq. (1) with

$$u=\frac{\partial \psi}{\partial y} \quad \text{and} \quad v=-\frac{\partial \psi}{\partial x} \tag{8}$$

Based on Eq. (8) with the similarity variables

$$\eta=y\sqrt{\frac{a}{\nu_f}},\ \psi=\sqrt{a\nu_f}xf(\eta), a=\frac{1}{s+bt},\ \theta(\eta)=\frac{T-T_\infty}{\frac{q_0x}{k_f}\sqrt{\frac{\nu_f}{a}}},$$

$$q(x)=q_0x, v_0(t)=v_i \tag{9}$$

b, s – a random constants, a – strength of squeezing flow, q_0 – heat flux, v_0 – the velocity at the sensor surface when permeable surfaces are considered. Based on the condition defined in Eq. (9), motion of channel's height is according to the following conditions: $h(t)=h_0/(s+bt)^{-\frac{1}{b}}$ for $b>0$ and $h(t)=h_0e^{-st}$ for $b=0$. The surface permeable velocity is expected to increase as the time decreases (when $b>0$) since squeezing velocities increase as time decreases.

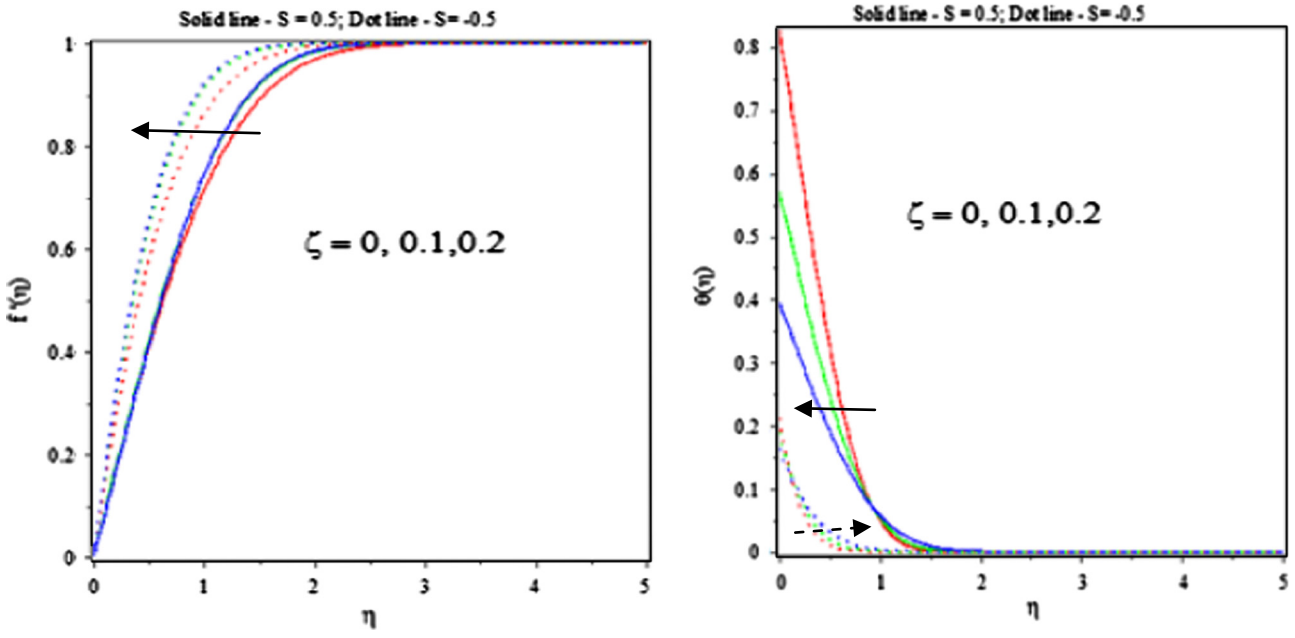

Figure 2 Comparison of nanoparticle volume fraction on velocity and temperature profiles, Rizwan et al. [35].

Table 2 Comparison of nanoparticle volume fraction on $f''(0)$.

Nanofluids	Parameter ζ	Num. method $f''(0)$	OHAM $f''(0)$	Error between Num. and OHAM
Cu–water	0.0	1.48113419 [35]	1.48113419 [35]	0.00000
	0.1	1.71105504	1.71105531	2.7E−07
	0.2	1.75138728	1.75138766	3.8E−07
Al_2O_3–water	0.0	1.48113419 [35]	1.48113419 [35]	0.00000
	0.1	1.43438455	1.43438501	4.6E−07
	0.2	1.33096758	1.33096794	3.6E−07
SWCNTs–water	0.0	1.48113419 [35]	1.48113419 [35]	0.00000
	0.1	1.45088235	1.45088232	3.0E−08
	0.2	1.35571879	1.35571877	2.0E−08

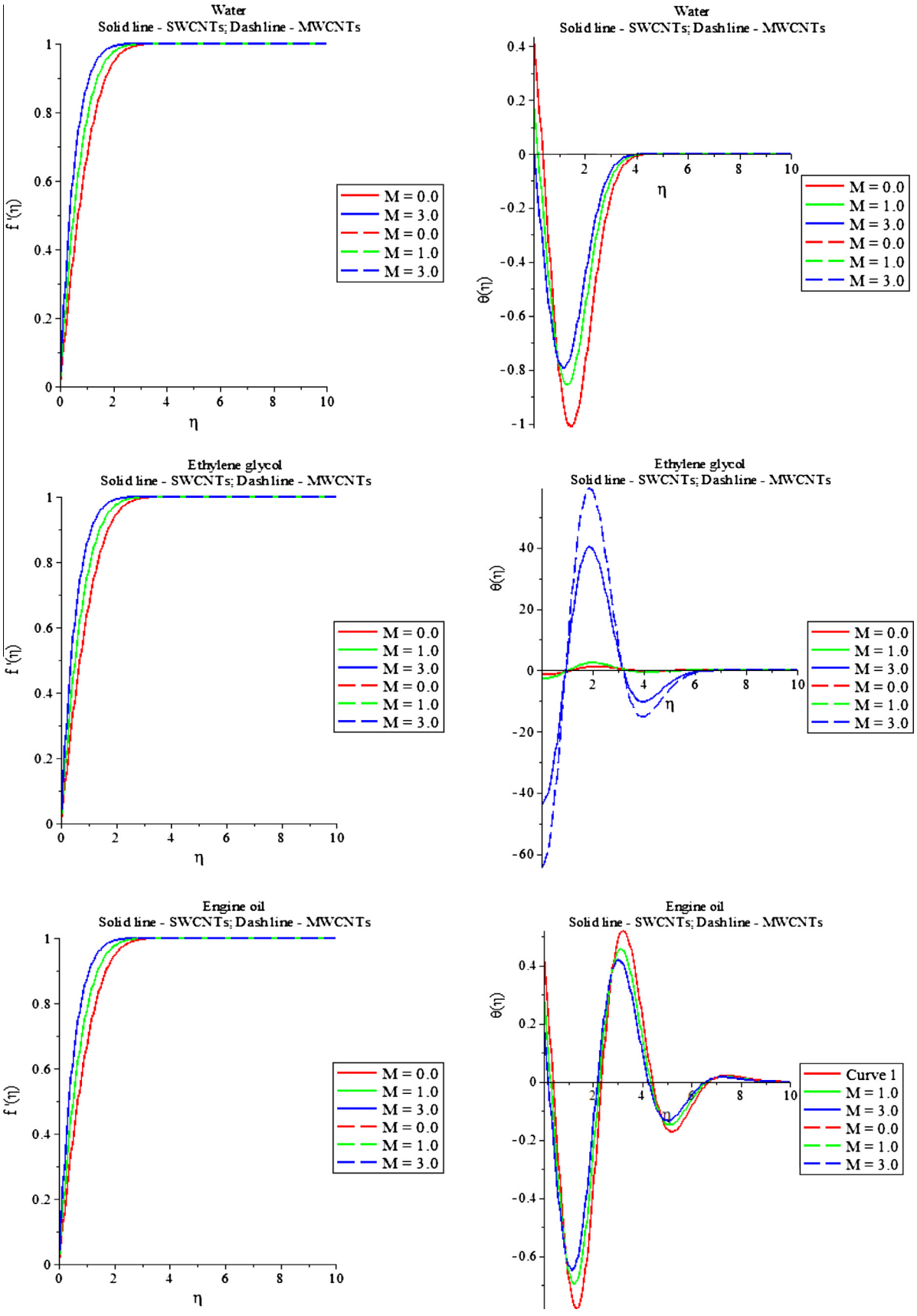

Figure 3 Magnetic effects on velocity and temperature profiles.

Eqs. (4) and (7) become

$$f''' + A1\left(\left(f + \frac{b\eta}{2}\right)f'' - f'^2 + b(f'^2 - 1) + \left(M\frac{A2}{A1} + \frac{\lambda}{A1}\right)(1 - f') + 1\right) = 0 \quad (10)$$

$$\frac{1}{Pr}\left(\frac{k_{nf}}{k_f A3} + \frac{Pr\ R}{k_f A3}\right)\theta'' + \left(\frac{\delta}{A3}\theta + \left(f + \frac{b\eta}{2}\right)\theta' - \left(f' + \frac{b}{2}\right)\theta\right) = 0 \quad (11)$$

with boundary conditions

$$f(0) = S, f'(0) = 0, \theta'(0) = -\frac{k_f}{k_{nf}};\ f'(\infty) \to 1, \theta(\infty) \to 0 \quad (12)$$

$$A_1 = (1-\zeta)^{2.5}\left(1 - \zeta + \zeta\frac{\rho_s}{\rho_f}\right), A_2 = (1-\zeta)^{2.5}\left(1 - \zeta + \zeta\frac{\sigma_s}{\sigma_f}\right),$$
$$A_3 = \left(1 - \zeta + \zeta\frac{(\rho c_p)_s}{(\rho c_p)_f}\right) \quad (13)$$

$Pr = \frac{(c_p\mu)_f}{k_f}$ – Prandtl number, $\delta = \frac{Q_0 x}{(\rho c_p)_f U}$ – heat source/sink parameter, $\lambda = \frac{\nu_f x}{UK}$ – porous parameter, $M = \frac{\sigma_f B_0^2 x}{U\rho_f}$ – magnetic parameter, $R = \frac{16\sigma_1\theta_w^3}{3k_f k^*}$ – thermal energy radiation parameter.

Physical quantities are $C_f = \frac{\tau_w}{\rho_f U^2}$ – skin friction coefficient, $Nu_x = \frac{q_w x}{k_f(T_w - T_\infty)}$ – local Nusselt number where τ_w and q_w are defined as

$$C_f(Re_x)^{1/2} = \frac{f''(0)}{(1-\zeta)^{2.5}}, \frac{Nu_x}{Re_x^{1/2}} = -\frac{k_{nf}}{k_f}\theta'(0) \quad (14)$$

$Re_x = \frac{Ux}{\nu_f}$ – the local Reynolds number.

3. Results and discussion

Calculations are performed by the OHAM (analytical method) and the fourth or fifth order Runge–Kutta Fehlberg method with shooting technique (numerical method) for different values of parameters. Eqs. (10) and (11) subjected to the boundary conditions (12) have been solved numerically and analytically using computer algebra software Maple 18 (Numeric) and Mathematica 5.2 (Analytic) respectively. For the benefit of the readers the solution proceeding by using fourth or fifth order Runge–Kutta Fehlberg method with shooting technique and the OHAM are listed in Appendix A. Throughout this calculation we have assumed $Pr = 6.2$ corresponds to nanofluids unless otherwise specified. In order to validate our methods, we have compared the results of $f''(0)$ with those of Rizwan et al. [35] and found them in good agreement, Table 2. Thermophysical properties of fluid and the nanoparticles are given in Table 1.

It is also observed from Fig. 2 and Table 2 that the agreement with the theoretical solution of the velocity and the temperature profiles and $f''(0)$ for different values of the nanoparticle volume fraction are correlated with Figs. 2a and 3a and Table 2 (water based Cu and Al_2O_3 when $\zeta = 0.0$) of Rizwan et al. [35]. In addition, we compare some of our results with the results of the previously published article, Rizwan et al. [35]. The comparisons are depicted in Table 2. A very excellent agreement can be observed between them.

Fig. 3 shows the effect of magnetic strength M on velocity and temperature profiles in the presence of water, ethylene glycol and engine oil based SWCNTs and MWCNTs over a horizontal sensor surface inside squeezed free stream. In all the three cases, it is observed that the velocity of the nanofluid increases whereas the temperature of the nanofluids near the wall decreases and then increases with increase of magnetic strength. This is due to the combined effect of electric and magnetic force along the squeezed nanofluids flow over a sensor surface. It is interesting to note that the temperature of MWCNTs-ethylene glycol attains its maximum and minimum value at $M = 3.0$ as compared to other mixtures whereas the temperature distribution of SWCNTs and MWCNTs – engine oil is having similar behavior with increase of magnetic strength. Application of a magnetic field moving with the squeezed free stream has the tendency to induce a motive force (Lorentz force) which slows down the motion of the nanofluid and firstly decreases and then increases its temperature profiles. For heat transfer characteristics mechanism of SWCNTs and MWCNTs in the presence of squeezed MHD flow, interesting result is the large distortion of the temperature field caused for $0.0 \leqslant M \leqslant 3$. The negative value of the temperature profile is seen in the outer boundary region for the combined strength of magnetic field and squeezed flow. It is interesting to note that the engine oil based MWCNTs play a dominant role on temperature distribution and heat transfer rate with increase of magnetic strength as compared to SWCNTS-engine oil, Table 3. It is also observed that the absence of magnetic strength $M = 0.0$ gives lower temperature distribution as compared to the presence of magnetic strength.

Table 3 Skin friction and rate of heat transfer for M with $\zeta = 0.01,\ b = 0.5,\ R = 0.5,\ Pr = 6.2,\ \delta = 0.5$.

Base fluid	M	SWCNTs		MWCNTs	
		$f''(0)$	$-\theta'(0)$	$f''(0)$	$-\theta'(0)$
Pure water	0.0	0.80002480	−0.42988652	0.79731397	−0.43373516
	1.0	1.19609816	−0.19110381	1.19473900	−0.19175889
	3.0	1.76399604	−0.01818228	1.76366081	−0.01774653
Ethylene glycol	0.0	0.79928134	1.209602281	0.79685252	1.212731332
	1.0	1.19572513	2.572116127	1.19450803	2.609461005
	3.0	1.76390412	43.55578724	1.76360376	64.24681393
Engine oil	0.0	0.80092035	−0.44003640	0.79787040	−0.43573987
	1.0	1.19654779	−0.30175609	1.19501781	−0.29668214
	3.0	1.76410676	−0.19315713	1.76372962	−0.18784897

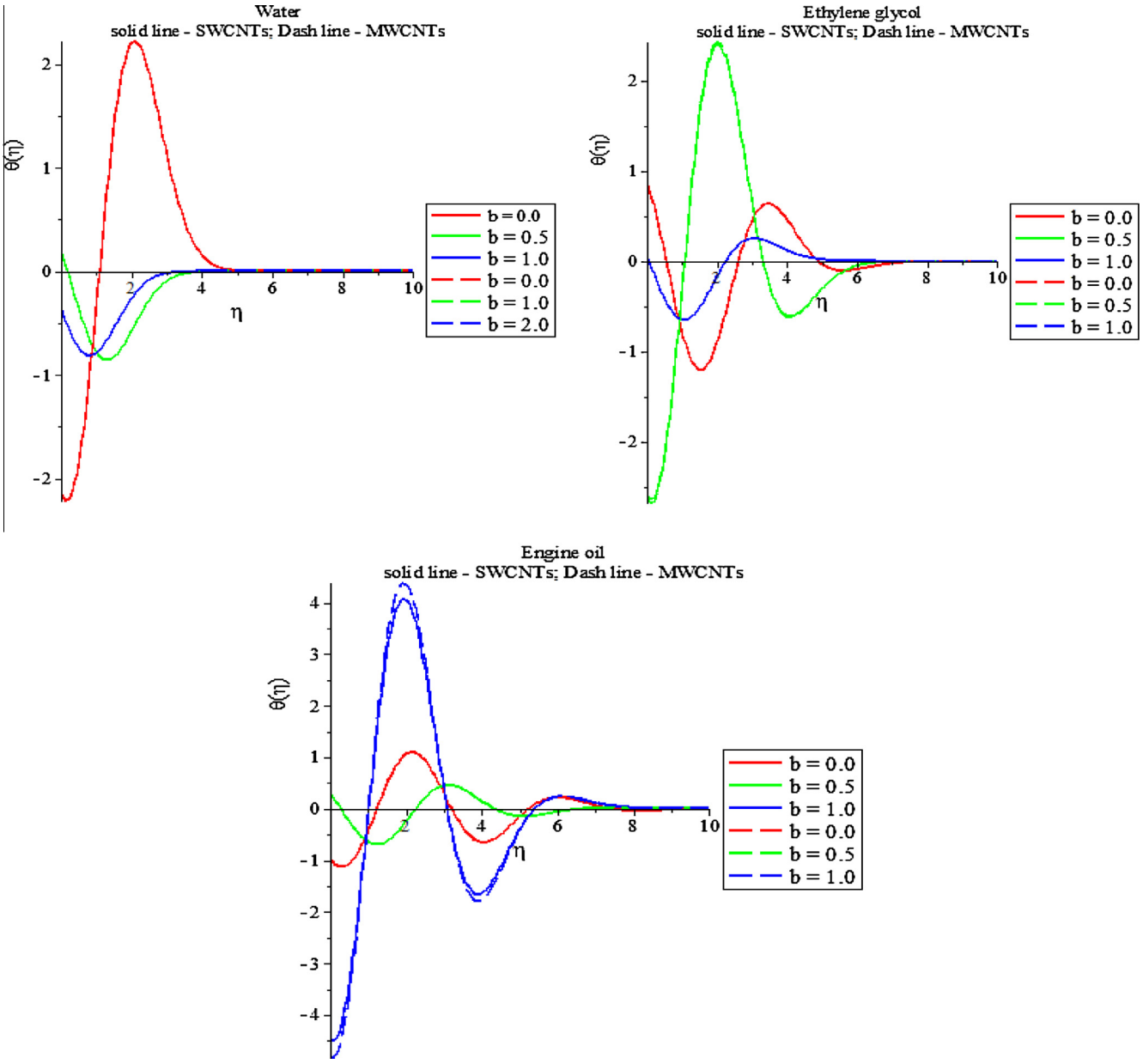

Figure 4 Squeezed parameter on velocity and temperature profiles.

In the presence of water, ethylene glycol and engine oil based SWCNTs and MWCNTs, it is noticed that the velocity of the nanofluids decreases as b increases causing the squeezed flow to be more attached to the horizontal sensor surface, Fig. 4. It is observed that the temperature of the water and engine oil based CNTs (SWCNTs and MWCNTs) firstly increases and then decreases whereas the temperature of ethylene glycol based CNTs firstly decreases and then increases with the increase of squeezed parameter. The negative value of the temperature profile is seen in the outer boundary region due to the joined effect of the thermal conductivity of the carbon nanotubes and the strength of the squeezed flow. It is also shown that the temperature distribution of water, ethylene glycol and engine oil based CNTs (SWCNTs and MWCNTs) attains its maximum value at squeezed number $b = 0.0$, $b = 0.5$ and $b = 1.0$ respectively. It is worth interesting to note that the engine oil based MWCNTs play a dominant role on temperature distribution and heat transfer rate with increase of squeezed parameter, Table 4. These results clearly demonstrate that the squeezed flow strength and shape of the CNTs can be used as a means of controlling the flow and heat transfer characteristics.

Effects of thermal radiation energy on water, ethylene glycol and engine oil based SWCNTs and MWCNTs are shown in Fig. 5. It is observed that the temperature of the nanofluids for ethylene glycol based CNTs (SWCNTs and MWCNTs) firstly decreases and then increases whereas the temperature of water and engine oil based CNTs decreases with increase of thermal radiation parameter, Fig. 5. According to Eqs. (2)–(4), the divergence of the radiative heat flux increases as thermal conductivity of the fluid (k_f) decreases which in turn increases the rate of radiative heat transferred to the nanofluids

Table 4 Skin friction and rate of heat transfer for b with $\zeta = 0.01,\ M = 1.0,\ R = 0.5,\ Pr = 6.2,\ \delta = 0.5$.

Base fluid	b	SWCNTs		MWCNTs	
		$f''(0)$	$-\theta'(0)$	$f''(0)$	$-\theta'(0)$
Pure water	0.0	1.15516266	1.533709168	1.15234378	1.526488384
	0.5	1.01406923	−0.27974455	1.01219270	−0.28130595
	1.0	0.86021045	0.281658319	0.85942071	0.280749973
Ethylene glycol	0.0	1.15438883	−1.12910036	1.15186467	−1.12007623
	0.5	1.01355429	1.783928885	1.01187354	1.798193049
	1.0	0.85999429	−0.11602670	0.85928598	−0.11472475
Engine oil	0.0	1.15609553	0.890256117	1.15929179	0.895663226
	0.5	1.01468978	−0.35528109	1.01257764	−0.35042338
	1.0	0.86047067	2.663507034	0.85958305	2.769969643

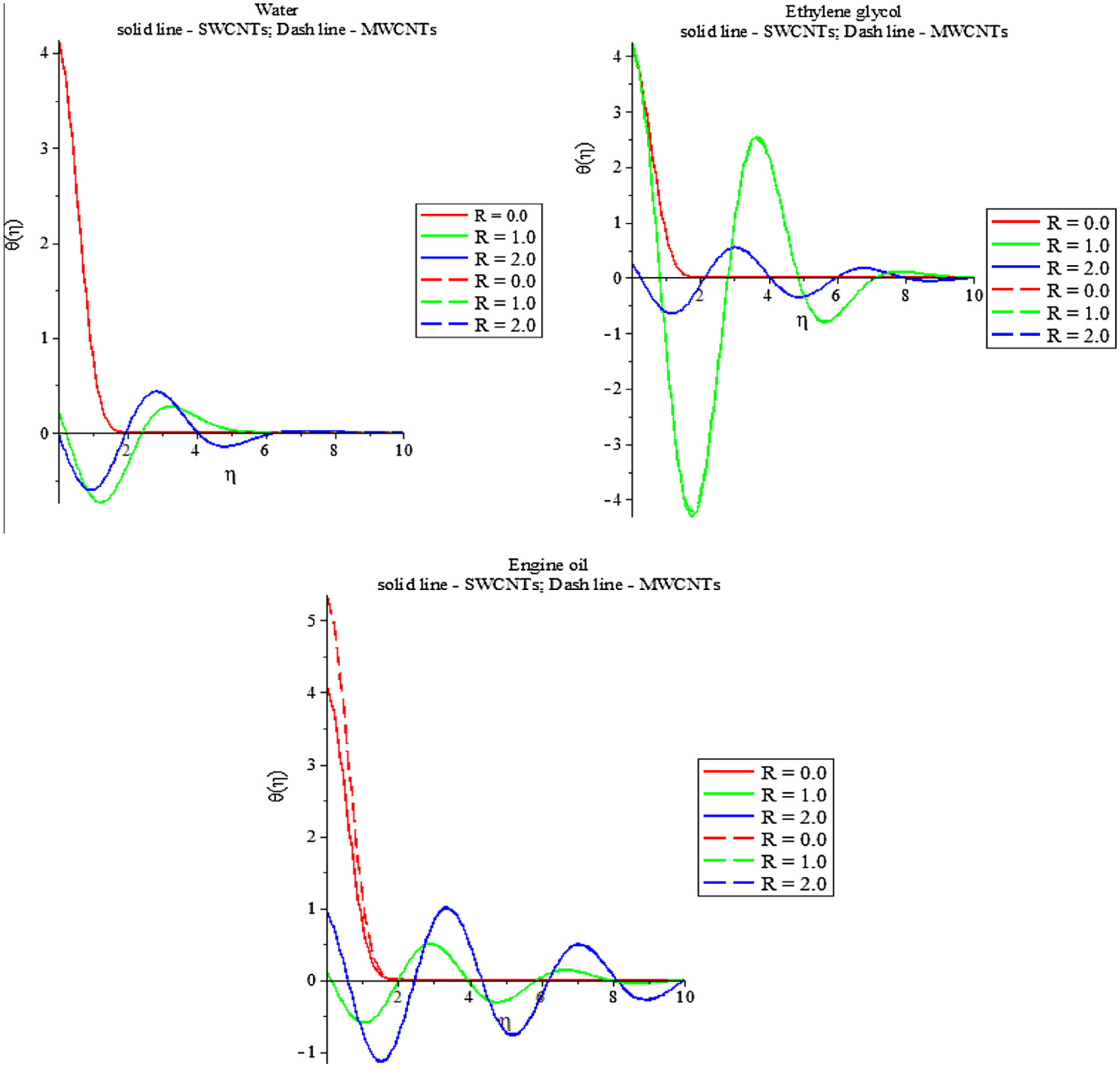

Figure 5 Thermal radiation energy on velocity and temperature profiles.

Table 5 Skin friction and rate of heat transfer for R with $\zeta = 0.01,\ b = 0.5,\ M = 1.0,\ Pr = 6.2,\ \delta = 0.5$.

Base fluid	R	SWCNTs		MWCNTs	
		$f''(0)$	$-\theta'(0)$	$f''(0)$	$-\theta'(0)$
Pure water	0.0	1.19609816	−4.12741719	1.19473908	−4.13636018
	1.0	1.19609816	−0.23435224	1.19473908	−0.23392784
	2.0	1.19609816	−0.18529160	1.19473908	−0.18331483
Ethylene glycol	0.0	1.19572513	−4.12113944	1.19450803	−4.12734846
	1.0	1.19572513	0.138403123	1.19450803	0.142957102
	2.0	1.19572513	−1.24682076	1.19450803	−1.23837101
Engine oil	0.0	1.19654778	−4.09830184	1.19501781	−4.10460673
	1.0	1.19654778	−0.22963335	1.19501781	−0.22580099
	2.0	1.19654778	0.212063249	1.19501781	0.212984755

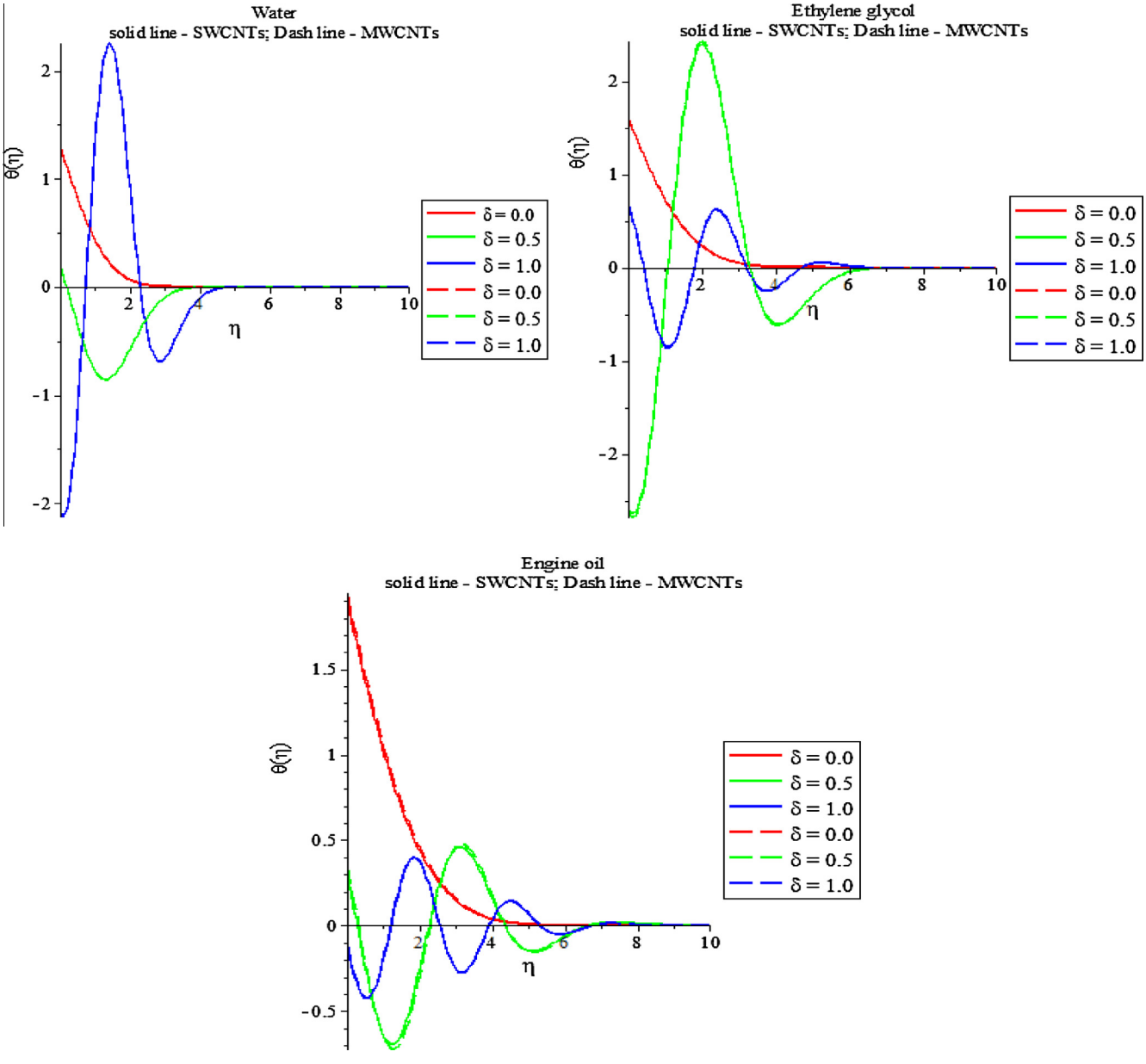

Figure 6 Heat source on velocity and temperature profiles.

Table 6 Skin friction and rate of heat transfer for δ with $\zeta = 0.01,\ b = 0.5,\ M = 1.0,\ Pr = 6.2,\ R = 0.5$.

Base fluid	δ	SWCNTs		MWCNTs	
		$f''(0)$	$-\theta'(0)$	$f''(0)$	$-\theta'(0)$
Pure water	0.1	1.19609816	−2.09957566	1.19473909	−2.10093444
	0.5	1.19609816	−0.19110381	1.19473909	−0.19175889
	1.0	1.19609816	2.082617587	1.19473909	2.083036473
Ethylene glycol	0.1	1.19572513	−6.06274385	1.19450803	−6.60638867
	0.5	1.19572513	−0.67417689	1.19450803	2.609461005
	1.0	1.19572513	−0.67417689	1.19450803	−0.66312124
Engine oil	0.1	1.19654779	3.913854858	1.19501781	3.921259038
	0.5	1.19654779	−0.30175609	1.19501781	−0.29668214
	1.0	1.19654779	0.116470377	1.19501781	0.118079800

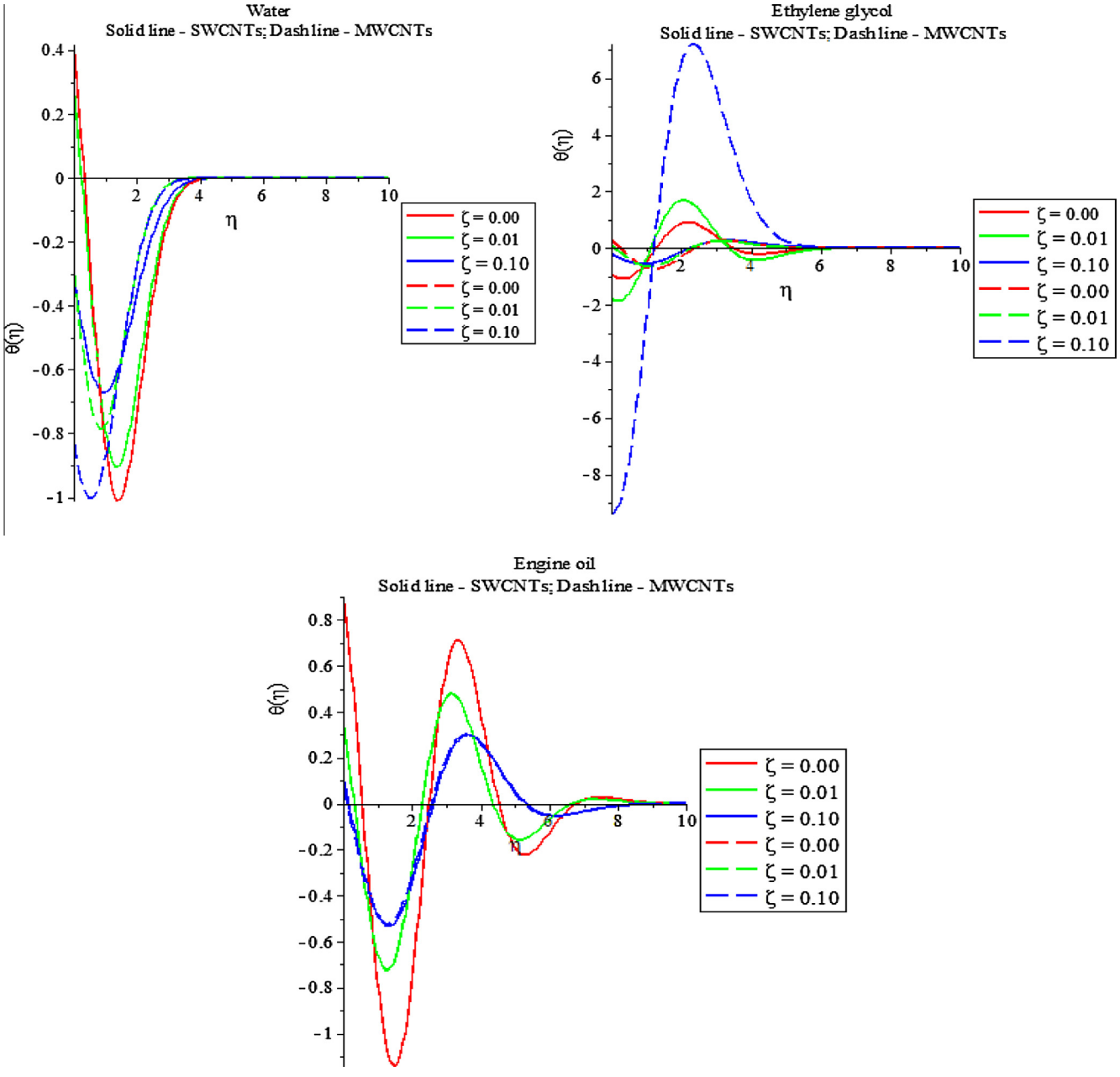

Figure 7 Nanoparticle volume fraction on temperature profiles.

Table 7 Skin friction and rate of heat transfer for ζ with $\delta = 0.5,\ b = 0.5,\ M = 1.0,\ Pr = 6.2,\ R = 0.5$.

Base fluid	δ	SWCNTs		MWCNTs	
		$f''(0)$	$-\theta'(0)$	$f''(0)$	$-\theta'(0)$
Pure water	0.0	1.02075698	−0.41576207	1.02075698	−0.41576207
	0.01	1.01406923	−0.27974455	1.01219270	−0.28130595
	0.1	0.95076169	0.302997930	0.93303549	0.294144017
Ethylene glycol	0.0	1.02075698	0.911181105	1.02075698	0.911181105
	0.01	1.01355429	1.783928885	1.01187354	1.798193049
	0.1	0.94599849	0.204300672	0.92991681	0.213042586
Engine oil	0.0	1.02075698	−0.90024335	1.02075698	−0.90024335
	0.01	1.01468978	−0.35528109	1.01257764	−0.35042338
	0.1	0.95640457	−0.11409495	0.93675590	−0.08229600

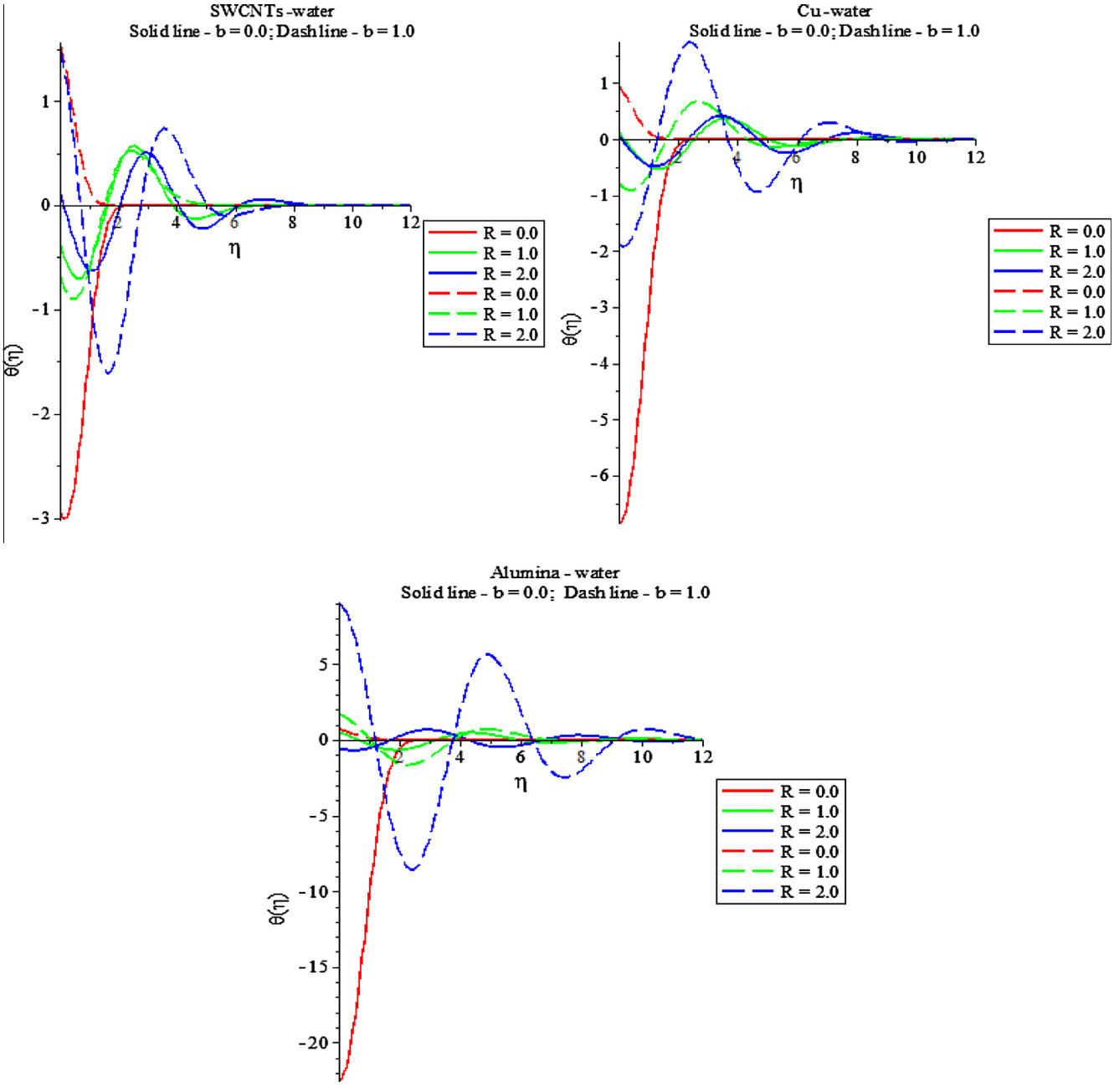

Figure 8 Thermal radiation energy on velocity and temperature profiles in the presence of squeezed parameter.

(water and engine oil based CNTs) and hence the squeezed nanofluid fluid flow temperature decreases. It is shown that the ethylene glycol and engine oil based CNTs (SWCNTs and MWCNTs) play a dominant role on temperature distribution with increase of thermal radiation energy. It is interesting to note that the engine oil based MWCNTs play an important role on heat transfer rate with increase of thermal radiation energy, Table 5. The increase in radiation parameter means the release of heat energy from the flow region and so the nanofluid temperature decreases as the thermal boundary layer thickness becomes thinner. All these physical behaviors are due to the combined effect of the strength of squeezed flow and size of the carbon nanotubes.

Effect of heat source ($\delta > 0$) on velocity and temperature distribution for water, ethylene glycol and engine oil based SWCNTs and MWCNTs is shown in Fig. 6. It is observed that the temperature of the water based CNTs (SWCNTs and MWCNTs) decreases, the temperature of the ethylene glycol based CNTs firstly decreases and then increases and the temperature of engine oil based CNTs firstly increases and then decreases with increase of heat source. The term $Q_0 (T_\infty - T)$ is assumed to be the amount of heat generated/absorbed per unit volume. Q_0 is a constant, which may take on either positive or negative values. When the wall temperature T_w exceeds the free stream temperature T_∞, the source term represents the heat source, $Q_0 > 0$ and heat sink, $Q_0 < 0$ whereas $T_w < T_\infty$,

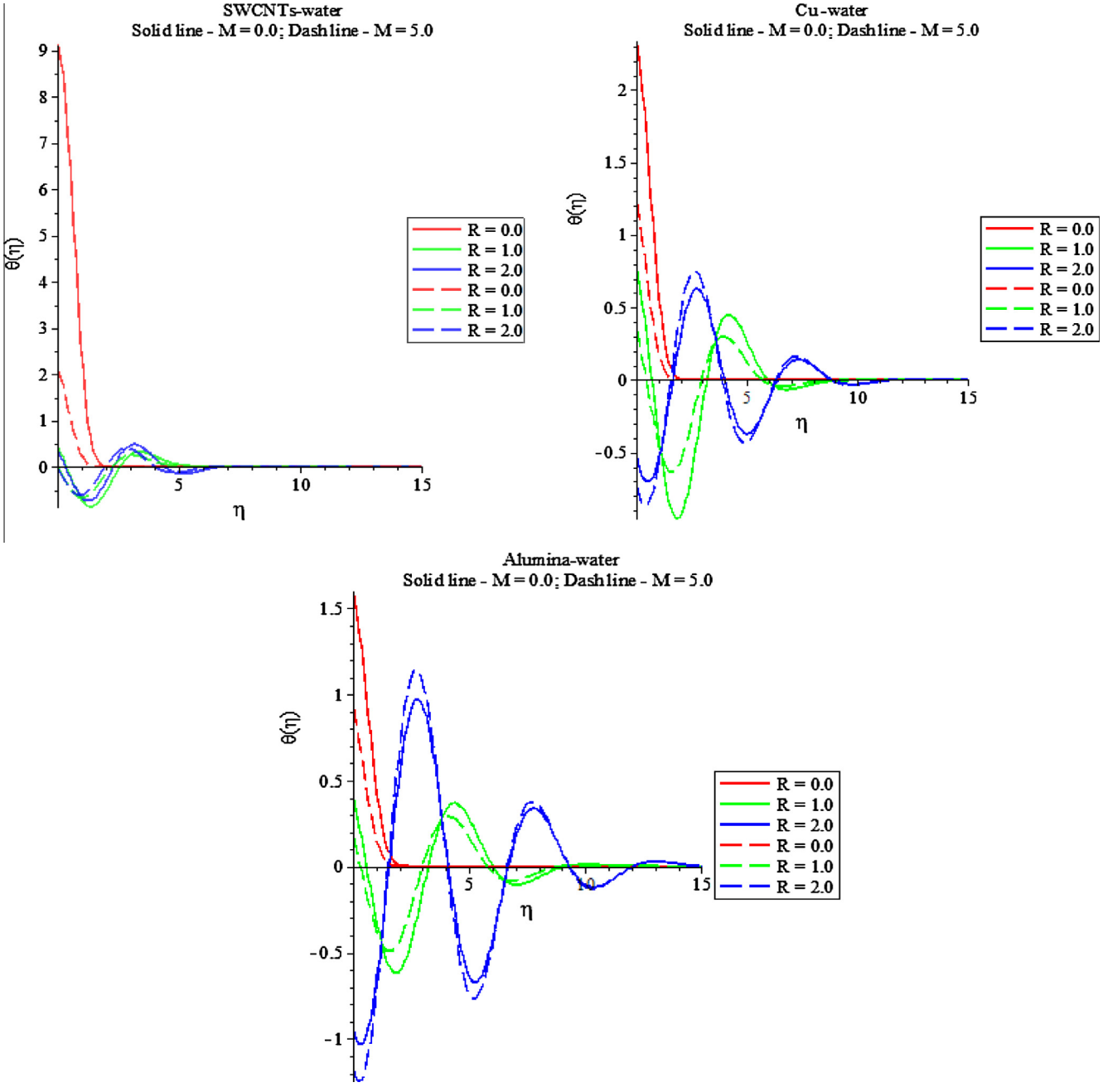

Figure 9 Thermal radiation energy on velocity and temperature profiles in the presence of magnetic field.

Table 8 Skin friction and rate of heat transfer for R with $\delta = 0.5,\ M = 1.0,\ Pr = 6.2$.

Nanofluid	R	$b = 0.0$		$b = 1.0$	
		$f''(0)$	$-\theta'(0)$	$f''(0)$	$-\theta'(0)$
SWCNTs–water	0.0	1.15516266	2.93600941	0.86021044	−1.56176558
	1.0	1.15516266	0.35822443	0.86021044	0.657986182
	2.0	1.15516266	1.74537298	0.86021044	−1.44416345
Cu–water	0.0	1.20368313	6.82641700	0.83679948	−0.95764950
	1.0	1.20368313	0.55214525	0.83679952	0.79078169
	2.0	1.20368313	−0.5425417	0.83679953	0.03874375
Alumina–water	0.0	1.10554196	22.5279262	0.79037468	−0.7415023
	1.0	1.10554196	0.67466216	0.79037471	−0.2581149
	2.0	1.10554196	0.07632537	0.79037471	0.31397641

Table 9 Skin friction and rate of heat transfer for R with $\zeta = 0.01,\ \delta = 0.5,\ b = 0.5,\ Pr = 6.2$.

Nanofluid	R	$M = 0.0$		$M = 5.0$	
		$f''^{(0)}$	$-\theta'(0)$	$f''(0)$	$-\theta'(0)$
SWCNTs–water	0.0	0.80002480	−9.12643015	2.20264041	−2.107132579
	1.0	0.80002480	−0.44550638	2.20264089	−0.010261692
	2.0	0.80002480	−0.36381091	2.20264089	0.0200652508
Cu–water	0.0	0.87637833	−2.33615385	1.98248263	−1.240001019
	1.0	0.87637833	−0.77390687	1.98248260	−0.364831868
	2.0	0.87637833	0.518039897	1.98248260	−0.720100869
Alumina–water	0.0	0.80658756	−1.59883911	1.86317000	−0.932112814
	1.0	0.80658758	−0.40712930	1.86316997	−0.189829245
	2.0	0.80658758	0.941596054	1.86316997	1.1700869083

the opposite relationship is true. Heat source generates energy which causes the temperature of the ethylene glycol based CNTs to decrease firstly and then increase in the boundary layer. It is interesting to note that the influence of internal heat generation on temperature distribution is more pronounced on the engine oil based CNTs than that of the other mixtures in the squeezed flow region. Increasing the heat source parameter δ has the tendency to up and down the thermal state of engine oil based MWCNTs, Table 6. All these physical behaviors are due to the combined effects of the strength of convective thermal radiation energy and the size and shape of the CNTs in the base fluids.

Fig. 7 displays the effects of volume fraction of the nanoparticles on velocity and temperature distribution in the presence of water, ethylene glycol and engine oil based SWCNTs and MWCNTs is shown in Fig. 7. In the presence of uniform squeezed flow, it is noted that the temperature of all the mixture decreases with increase of the nanoparticle volume fraction parameter ζ. This agrees with the physical behavior that when the volume fraction of CNTs increases the thermal conductivity and then the thermal boundary layer thickness increase. It is interesting to note that the temperature of the engine oil CNTs decreases near the wall and then increases whereas the rate of heat transfer of engine oil based MWCNTs is stronger than that of SWCNTs with increase of nanoparticle volume fraction, Table 7. Changes in the size, shape, material, and volume fraction of the CNTs allow for tuning to maximize spectral absorption of thermal energy throughout the nanofluid volume because the nanoparticle volume fraction parameter depends on the size and shape of the CNTs.

Effect of thermal radiation energy on the water based Cu, Al_2O_3 and SWCNTs in the presence of $b = 0.0, 1.0$ and $M = 0.0, 5.0$ is shown in Figs. 8 and 9. In both the cases, it is shown that the velocity of the nanofluids is uniform with increase of thermal radiation energy. In the presence of squeezed flow (b = 1.0), it is observed that the temperature distribution of SWCNTs–water is stronger than Cu–water and Al_2O_3–water with increase of thermal radiation. In the presence of magnetic field, it is noted that the temperature of the water based SWCNTs, Cu and Al_2O_3 decreases near the wall and then increases with increase of thermal radiation. It is interesting to note that the temperature distribution of Al_2O_3–water attains its maximum and minimum value at $R = 2.0, M = 5.0$ as compared to the other mixtures in the flow region. In the presence of squeezed parameter, b = 1.0, the rate of heat transfer of Al_2O_3–water increases whereas the rate of heat transfer of water based SWCNTs and Cu firstly increases and then decreases with increase of thermal radiation, Table 8. In the presence of magnetic strength, M = 5.0, the rate of heat transfer of nanofluids (water based Cu, Al_2O_3 and SWCNTs) increases with increase of thermal radiation energy whereas the thermal boundary layer thickness of squeezed SWCNTS–water is stronger as compared to the other mixtures in the flow region, Table 9.

4. Conclusion

Performance of thermal radiation energy of water, ethylene glycol and engine oil based Cu, Al_2O_3 and CNTs (SWCNTs and MWCNTs) is examined between squeezing surfaces in such a way that upper plate is squeezed. Comparison of temperature and the rate of heat transfer among the nanofluids with different parameters is presented in terms of Figures and Tables using Maple 18 (Numerical technique) and Mathematica 5.2 (OHAM). Conclusion remarks of the convergent results are as follows:

- Ethylene glycol based MWCNTs play a dominant role on temperature distribution and the rate of heat transfer with increase of magnetic strength as compared to other mixtures in the squeezed flow region.
- In the presence of squeezed parameter, $b = 1.0$ the temperature distribution of engine oil based MWCNTs attains its maximum and minimum values as compared to the other mixtures.
- The effect of thermal radiation energy is to reduce the temperature of engine oil based CNTs (SWCNTs and MWCNTs) significantly in the squeezed flow region.
- The influence of internal heat generation on temperature distribution is more pronounced on the engine oil based CNTs than on the other mixtures in the squeezed flow region over a sensor surface.
- The temperature of the engine oil based CNTs decreases near the wall and then increases with increase of nanoparticle volume fraction because the nanoparticle volume fraction depends on the size and shape of the CNTs.
- Enhancement in thermal conductivity can lead to efficiency improvements on the engine oil based CNTs heat transfer rate.
- In the presence of thermal radiation energy, the squeezed SWCNTs–water and the high magnetic strength of water based Al_2O_3 plays a dominant role on temperature distribution as compared to other mixtures in the flow region over a sensor surface.

Carbon nanotubes are superb materials for nanoscale thermal management applications, due to their extremely high thermal conductivity and quasi-one-dimensional geometry. Squeeze MHD flow of engine oil based CNTs between surfaces is important in rheology, material processing, lubrication and biomedical applications.

Appendix A

A.1. Numerical solution

Eqs. (10) and (11) subjected to the boundary condition (12) are converted into the following simultaneous system of first order differential equations as follows:

$$A_1 = (1-\zeta)^{2.5}\left(1-\zeta+\zeta\frac{\rho_s}{\rho_f}\right),\ A_2 = (1-\zeta)^{2.5}\left(1-\zeta+\zeta\frac{\sigma_s}{\sigma_f}\right),$$

$$A_3 = \left(1-\zeta+\zeta\frac{(\rho c_p)_s}{(\rho c_p)_f}\right),\ A_4 = (1-\zeta),$$

$$A_5 = \left(\frac{k_{nf}}{k_f A3}+\frac{Pr\ R}{k_f A3}\right) \tag{15}$$

$$f'(\eta) = u(\eta),\ u'f(\eta) = v(\eta),$$
$$v'(\eta) = -A1\left(\left(f+\frac{b\eta}{2}\right)f'' - f'^2 + b(f'^2-1) + \left(M\frac{A2}{A1}+\frac{\lambda}{A1}\right)(1-f') + 1\right) \tag{16}$$

$$\theta'(\eta) = p(\eta),\ p'(\eta) = -\frac{Pr}{A_5}\left(\frac{\delta}{A3}\theta + \left(f+\frac{b\eta}{2}\right)\theta' - \left(f'+\frac{b}{2}\right)\theta\right) \tag{17}$$

The boundary conditions are as follows:

$$f(0) = S, u(0) = 0, p(0) = -\frac{k_f}{k_{nf}}; u(L) = 1, \theta(L) = 0,$$
$$v(0) = \alpha, \theta(0) = \beta \tag{18}$$

where α and β are priori unknowns to be determined as a part of the solution.

This software uses a fourth–fifth order Runge–Kutta–Fehlberg method with shooting technique as default to solve the boundary value problems numerically using the Dsolve command MAPLE 18. The values of α and β are determined upon solving the boundary conditions $v(0) = \alpha$, $\theta(0) = \beta$ with trial and error basis. The numerical results are represented in the form of the dimensionless velocity and temperature in the presence of water, ethylene glycol and engine oil based CNTs, Cu and Al_2O_3.

A.2. Analytical solution using optimal homotopy asymptotic method (OHAM)

Based on the optimal homotopy asymptotic method, the nonlinear ordinary differential Eqs. (8)–(10) with boundary conditions (12) can be assumed as

$$f = f_0 + pf_1 + p^2 f_2,\ \theta = \theta_0 + p\theta_1 + p^2\theta_2 \text{ and}$$
$$H_1(p) = pC_1 + p^2C_2,\ H_2(p) = pC_3 + p^2C_4$$

where $p \in [0,1]$ is an embedding parameter, H_p is a nonzero auxiliary function, and C_i are constants [34].

A.2.1. Approximation of the momentum boundary layer problem

Based on the optimal homotopy asymptotic method, Eq. (10) and the boundary conditions (12) can be written as

$$L = f'' + f' \quad \text{and}$$
$$N = f''' + A1\left(\left(f+\frac{b\eta}{2}\right)f'' - f'^2 + b(f'^2-1) + \left(M\frac{A2}{A1}+\frac{\lambda}{A1}\right)(1-f') + 1\right) - f'' - f' \tag{19}$$

L and N be the linear operator and the nonlinear operator. After applied OHAM to the Eq. (8) with respect to Eq. (12), we have

$$(1-p)[f''+f'] = H_p\left[f''' + A1\left(\left(f+\frac{b\eta}{2}\right)f'' - f'^2 + b(f'^2-1) + \left(M\frac{A2}{A1}+\frac{\lambda}{A1}\right)(1-f') + 1\right)\right] \tag{20}$$

The zeroth-order equation p^0 of the boundary condition is

$$f_0''+f_0'=0,\ f_0(0)=S,\ f_0'(0)=0 \tag{21}$$

The solution of the zeroth-order equation is

$$f_0(\xi)=-\frac{e^{-\xi}(1-e^{\xi}+n-ne^{\xi}-\alpha e^{\xi}+\alpha ne^{\xi})}{1+n} \tag{22}$$

The first-order equation p^1 is

$$\begin{aligned} f_1''+f_1' &= f_0''+f_0'+C_1\left[f_0'''+A1\left(\left(f_0+\frac{b\eta}{2}\right)f_0''-f_0'^2+b\left(f_0'^2-1\right)\right.\right.\\ &\left.\left.+\left(M\frac{A2}{A1}+\frac{\lambda}{A1}\right)(1-f_0')+1\right)\right]\\ f_1(0)&=0,\ f_1'(0)=0 \end{aligned} \tag{23}$$

The second-order equation p^2 is

$$\left\{\begin{array}{c} f_2''+f_2'=f_1''+f_1'+C_1\left[f_1'''+A1\left(\left(f_1+\frac{b\eta}{2}\right)f_1''-2f_0'f_1'+2bf_0'f_1'-2f_0'f_1'\left(M\frac{A2}{A1}+\frac{\lambda}{A1}\right)\right)\right]\\ +C_2\left[f_0'''+A1\left(\left(f_0+\frac{b\eta}{2}\right)f_0''-f_0'^2+b\left(f_0'^2-1\right)+\left(M\frac{A2}{A1}+\frac{\lambda}{A1}\right)(1-f_0')+1\right)\right],\ f_2(0)=0,\ f_2'(0)=0 \end{array}\right\} \tag{24}$$

Solving the Eqs. (23) and (24) with the boundary conditions with the help of Eq. (22), then the solution of Eq. (10) can be determined approximately in the form of

$$f(\xi)=f_0(\xi)+f_1(\xi)+f_2(\xi) \tag{25}$$

Therefore the residual equation becomes

$$\begin{aligned} R_1(\xi,C_1,C_2)=&\left[f'''(\xi)+A1\left(\left(f(\xi)+\frac{b\xi}{2}\right)f''(\xi)-f'^2(\xi)\right.\right.\\ &\left.\left.+b(f'^2(\xi)-1)+\left(M\frac{A2}{A1}+\frac{\lambda}{A1}\right)(1-f'(\xi))+1\right)\right] \end{aligned} \tag{26}$$

The constants C_1 and C_2 can be optimally identified from the following conditions:

$$\frac{\partial J_1}{\partial C_1}=\frac{\partial J_1}{\partial C_2}=0 \quad \text{where} \quad J_1(C_i)=\int_0^{\infty}R_1^2(\xi,C_i)d\xi \tag{27}$$

A.2.2. Approximation of the energy boundary layer problem

Based on the optimal homotopy asymptotic method, Eq. (9) with the boundary condition (11) can be applied as

$L=(\theta'+\theta)$ and

$$N=\theta''+\frac{Pr}{A_5}\left(\frac{\delta}{A3}\theta+\left(f+\frac{b\eta}{2}\right)\theta'-\left(f'+\frac{b}{2}\right)\theta\right)-(\theta'+\theta)$$

L and N – the nonlinear operator. Again by OHAM on Eq. (9) with respect to Eq. (11), we have

$$(1-p)[\theta'+\theta]=H_p\left[\theta''+\frac{Pr}{A_5}\left(\frac{\delta}{A3}\theta+\left(f+\frac{b\eta}{2}\right)\theta'-\left(f'+\frac{b}{2}\right)\theta\right)\right] \tag{28}$$

The zeroth-order equation p^0 is

$$(\theta_0'+\theta_0)=0,\ \theta_0(0)=1 \tag{29}$$

Therefore the solution of zeroth-order equation is

$$\theta_0(\xi)=e^{-\xi} \tag{30}$$

The first-order equation p^1 is

$$\begin{aligned} \theta_1'+\theta_1 &= \theta_0'+\theta_0+C_3\left[\theta_0''+\frac{Pr}{A_5}\left(\frac{\delta}{A3}\theta_0+\left(f_0+\frac{b\eta}{2}\right)\theta_0'\right.\right.\\ &\left.\left.-\left(f_0'+\frac{b}{2}\right)\theta_0\right)\right],\theta_1(0)=0 \end{aligned} \tag{31}$$

The second-order equation p^2 is

$$\left\{\begin{array}{c} \theta_2'+\theta_2=\theta_1'+\theta_1+C_3\left[\theta_1''+\frac{Pr}{A_5}\left(\frac{\delta}{A3}\theta_1+\left(f_0+\frac{b\eta}{2}\right)\theta_1'+\left(f_1+\frac{b}{2}\right)\theta_0'-\left(f_0'+\frac{b}{2}\right)\theta_1\right)-\left(f_1'\right)\theta_0\right]\\ +C_4\left[\theta_0''+\frac{Pr}{A_5}\left(\frac{\delta}{A3}\theta_0+\left(f_0+\frac{b\eta}{2}\right)\theta_0'-\left(f_0'+\frac{b}{2}\right)\theta_0\right)\right],\ \theta_2(0)=0 \end{array}\right\} \tag{32}$$

Solving the Eqs. (31) and (32) with the boundary conditions with the help of Eq. (30), the solution of Eq. (11) can be determined approximately as

$$\theta(\xi)=\theta_0(\xi)+\theta_1(\xi)+\theta_2(\xi) \tag{33}$$

The residual equation becomes

$$\begin{aligned} &R_2(\xi,C_3,C_4)\\ &=\left[\theta''(\xi)+\frac{Pr}{A_5}\left(\frac{\delta}{A3}\theta(\xi)+\left(f(\xi)+\frac{b\xi}{2}\right)\theta'(\xi)-\left(f'(\xi)+\frac{b}{2}\right)\theta(\xi)\right)\right] \end{aligned}$$

The constants C_3 and C_4 can be optimally derived from

$$\frac{\partial J_2}{\partial C_3}=\frac{\partial J_2}{\partial C_4}=0 \quad \text{where} \quad J_2(C_i)=\int_0^{\infty}R_2^2(\xi,C_i)d\xi \tag{35}$$

The results obtained for $f''(0)$ in this work, are compared with the solutions obtained in Rizwan et al. [35], for validation purposes, Table 2.

References

[1] J.C. Maxwell, Electricity and Magnetism, third ed., Clarendon, Oxford, England, UK, 1904.
[2] R.L. Hamilton, O.K. Crosser, Thermal conductivity of heterogeneous two component systems, Ind. Eng. Chem. Fundam. 1 (3) (1962) 187–191.
[3] E.J. Wasp, J.P. Kenny, R.L. Gandhi, Solid-Liquid Flow Slurry Pipeline Transportation, Bulk Materials Handling, vol. 1, no. 4, Trans. Tech. Publications, Clausthal, Germany, 1977.
[4] S.U.S. Choi, Enhancing thermal conductivity of fluids with nanoparticle, in: D.A. Siginer, H.P. Wang (Eds.), Developments and Applications of Non-Newtonian Flows, vol. 231, ASME, 1995, pp. 99–105.
[5] S.U.S. Choi, Z.G. Zhang, W. Yu, F.E. Lockwood, E.A. Grulke, Anomalously thermal conductivity enhancement in nanotube suspensions, Appl. Phys. Lett. 79 (2001) 2252–2254.
[6] J. Buongiorno, Convective transport in nanofluids, ASME J. Heat Transf. 128 (2006) 240–250.
[7] T.C. Papanastasiou, G.C. Georgiou, A.N. Alexandrou, Viscous Fluid Flow, CRC Press, New York, NY, USA, 1994.
[8] M.J. Stefan, Versuch Uber die scheinbare adhesion, Akademie der Wissenschaften 69 (1874) article 713.
[9] X.J. Ran, Q.Y. Zhu, Y. Li, An explicit series solution of the squeezing flow between two infinite parallel plates, Commun. Nonlinear Sci. Numer. Simul. 8 (2007) 179–184.
[10] R.J. Grimm, Squeezing flows of Newtonian liquid films an analysis including fluid inertia, Appl. Sci. Res. 32 (1976) 149–166.
[11] W.F. Hughes, R.A. Elco, Magnetohydrodynamic lubrication flow between parallel rotating disks, J. Fluid Mech. 13 (1962) 21–32.
[12] S. Kamiyama, Inertia effects in MHD hydrostatic thrust bearing, J. Tribol. 91 (1969) 589–596.
[13] E.A. Hamza, The magnetohydrodynamic squeeze film, J. Tribol. 110 (1988) 375–377.
[14] S. Bhattacharyya, A. Pal, Unsteady MHD squeezing flow between two parallel rotating discs, Mech. Res. Commun. 24 (1997) 615–623.
[15] R.L. Verma, A numerical solution for squeezing flow between parallel channels, Wear 72 (1981) 89–95.
[16] P. Singh, V. Radhakrishnan, K.A. Narayan, Squeezing flow between parallel plates, Ingénieur-Arch. 60 (1990) 274–281.
[17] P.J. Leider, R.B. Bird, Squeezing flow between parallel disks. I. Theoretical analysis, Ind. Eng. Chem. Fundam. 13 (1973) 336–341.
[18] N.B. Naduvinamani, P.S. Hiremath, G. Gurubasavaraj, Squeeze film lubrication of a short porous journal bearing with couple stress fluids, Tribol. Int. 34 (2001) 739–747.
[19] A. Qayyum, M. Awais, A. Alsaedi, T. Hayat, Flow of Jeffery fluid between two parallel disks, Chin. Phys. Lett. 29 (2012) 034701.
[20] R.J. Grimm, Squeezing flows of Newtonian liquid films an analysis include the fluid inertia, Appl. Sci. Res. 32 (1976) 149–166.
[21] J.A. Tichy, W.O. Winer, Inertial considerations in parallel circular squeeze film bearings, J. Lubr. Technol. 92 (1970) 588–592.
[22] H.M. Laun, M. Rady, O. Hassager, Analytical solutions for squeeze flow with partial wall slip, J. NonNewtonian Fluid Mech. 81 (1999) 1–15.
[23] S. Ishizawa, The unsteady flow between two parallel discs with arbitrary varying gap width, Bull. Jpn. Soc. Mech. Eng. 9 (1966) 533–550.
[24] P. Kim, L. Shi, A. Majumdar, P.L. McEuen, Thermal transport measurements of individual multiwalled nanotubes, Phys. Rev. Lett. 87 (21) (2001) 215502.
[25] S. Iijima, Helical microtubules of graphitic carbon, Nature 354 (1991) 56–58.
[26] M. Das, R. Mahato, R. Nandkeolyar, Newtonian heating effect on unsteady hydromagnetic Casson fluid flow past a flat plate with heat and mass transfer, Alexandria Eng J. 54 (2015) 871–879.
[27] S. Das, R.N. Jana, Natural convective magneto-nanofluid flow and radiative heat transfer past a moving vertical plate, Alexandria Eng. J. 54 (2015) 55–64.
[28] Samir Kumar Nandy, Sumanta Sidui, Tapas Ray Mahapatra, Unsteady MHD boundary-layer flow and heat transfer of nanofluid over a permeable shrinking sheet in the presence of thermal radiation, Alexandria Eng. J. 53 (2014) 929–937.
[29] Noreen Sher Akbar, S. Nadeem, Zafar Hayat Khan, Numerical simulation of peristaltic flow of a Carreau nanofluid in an asymmetric channel, Alexandria Eng J. 53 (2014) 191–197.
[30] S.K. Parida, S. Panda, B.R. Rout, MHD boundary layer slip flow and radiative nonlinear heat transfer over a flat plate with variable fluid properties and thermophoresis, Alexandria Eng. J. 54 (2015) 941–953.
[31] R. Ellahi, M. Hassan, A. Zeeshan, Study on magnetohydrodynamic nanofluid by means of single and multi-walled carbon nanotubes suspended in a salt water solution, IEEE Trans. Nanotechnol. 14 (2015) 726–734.
[32] M. Sheikholeslami, R. Ellahi, Simulation of ferrofluid flow for magnetic drug targeting using Lattice Boltzmann method, Zeitschrift für Naturforschung A 70 (2) (2015) 115–124.
[33] N.S. Akbar, M. Raza, R. Ellahi, Influence of induced magnetic field and heat flux with the suspension of carbon nanotubes for the peristaltic flow in a permeable channel, J. Magn. Magn. Mater. 381 (2015) 405–415.
[34] R. Ellahi, M. Hassan, A. Zeeshan, Shape effects of nanosize particles in Cu–H_2O nanofluid on entropy generation, Int. J. Heat Mass Transf. 81 (2015) 449–456.
[35] Rizwan Ul Hag, S. Nadeem, Z.H. Khan, N.F.M. Noor, MHD squeezed flow of water functionalized metallic nanoparticles over a sensor surface, Physica E 73 (2015) 45–53.
[36] Chaoli Zhang, Liancun Zheng, Xinxin Zhang, Goong Chen, MHD flow and radiation heat transfer of nanofluids in porous media with variable surface heat flux and chemical reaction, Appl. Math. Model. 39 (2015) 165–181.
[37] S. Rashidi, M. Dehghan, R. Ellahi, M. Riaz, M.T. Jamal-Abad, Study of stream wise transverse magnetic fluid flow with heat transfer around a porous obstacle, J. Magn. Magn. Mater. 378 (2015) 128–137.
[38] M.M. Rahman, I.A. Eltayeb, Radiative heat transfer in a hydromagnetic nanofluid past a non-linear stretching surface with convective boundary condition, Meccanica 48 (2013) 601–615.
[39] Ali J. Chamkha, A.M. Rashad, Abdelraheem M. Aly, Transient natural convection flow of a nanofluid over a vertical cylinder, Meccanica 48 (2013) 71–81.
[40] Saeed Dinarvand, Reza Hosseini, Ebrahim Damangir, Ioan Pop, Series solutions for steady three-dimensional stagnation point flow of a nanofluid past a circular cylinder with sinusoidal radius variation, Meccanica 48 (2013) 643–652.
[41] Ali J. Chamkha, S. Abbasbandy, A.M. Rashad, Radiation effects on mixed convection about a cone embedded in a porous medium filled with a nanofluid, Meccanica 48 (2013) 275–285.

[42] M.M. Rashidi, N. Freidoonimehr, A. Hosseini, O. Anwar Bég, T.-K. Hung, Homotopy simulation of nanofluid dynamics from a non-linearly stretching isothermal permeable sheet with transpiration, Meccanica 49 (2014) 469–482.
[43] A.R.A. Khaled, K. Vafai, Hydromagnetic squeezed flow and heat transfer over a sensor surface, Int. J. Eng. Sci. 42 (2004) 509–519.
[44] J.C. Maxwell, A Treatise on Electricity and Magnetism, second ed., Clarendon Press, Oxford, UK, 1881.
[45] J.C. Maxwell, A Treatise on Electricity and Magnetism, Oxford University Press, London, 1904, pp. 435–441.
[46] Dulal Pal, Gopinath Mandal, Influence of thermal radiation on mixed convection heat and mass transfer stagnation-point flow in nanofluids over stretching/shrinking sheet in a porous medium with chemical reaction, Nucl. Eng. Des. 273 (2014) 644–652.